applied optics

Simplified optical correlation-domain reflectometry without reference path

Makoto Shizuka,[1] Neisei Hayashi,[2] Yosuke Mizuno,[1,*] and Kentaro Nakamura[1]

[1]Laboratory for Future Interdisciplinary Research of Science and Technology, Tokyo Institute of Technology, 4259, Nagatsuta-cho, Midori-ku, Yokohama 226-8503, Japan
[2]Research Center for Advanced Science and Technology, The University of Tokyo, 4-6-1, Komaba, Meguro-ku, Tokyo 153-8904, Japan
*Corresponding author: ymizuno@sonic.pi.titech.ac.jp

Received 7 March 2016; revised 17 April 2016; accepted 21 April 2016; posted 21 April 2016 (Doc. ID 260502); published 12 May 2016

We develop a simplified configuration for optical correlation-domain reflectometry (OCDR) without an explicit reference path. Instead, the Fresnel-reflected light generated at the distal open end of the sensing fiber is exploited as a reference light. After the fundamental demonstration, the optimal incident power is found to be approximately 8 dBm. We also show that the loss near the distal end should not be applied, unlike in the case of Brillouin-based OCDR.

OCIS codes: (060.2370) Fiber optics sensors; (120.1840) Densitometers, reflectometers; (120.5700) Reflection.

http://dx.doi.org/10.1364/AO.55.003925

1. INTRODUCTION

Fiber-optic reflectometry is a fundamental technique for implementing multiplexed and distributed sensing systems [1–8], and its various configurations have been developed to detect a variety of physical parameters, such as strain [2–4], temperature [3–6], pressure [7], and humidity [8]. Among these various configurations, in order to detect bad connections (or splices) and other reflection points along fibers under test (FUTs) in a distributed manner, three types of fiber-optic reflectometry based on Fresnel reflection have been developed: optical time-domain reflectometry (OTDR) [9–13], optical frequency-domain reflectometry (OFDR) [14–18], and optical correlation (or coherence)-domain reflectometry (OCDR) [19–28]. It has been reported that OTDR commonly suffers from a relatively low spatial resolution and a low sampling rate, while OFDR generally suffers from phase fluctuations caused by environmental disturbances. Thus, here we focus on OCDR, which can mitigate these shortcomings.

OCDR operates by exploiting a synthesized optical coherence function (SOCF) [26]—i.e., by controlling the correlation of propagating light beams through optical frequency modulation. The modulation methods can be broken into two categories: sinusoidal modulation [21–23] and stepwise modulation [24–26] (including frequency-comb-based modulation [27,28]). As the latter approach requires accurate frequency adjustment and/or frequency-comb generation, sinusoidal modulation is more cost-efficient [21–23]. In a standard SOCF-OCDR system [21–28], an optical frequency shifter such as an acousto-optic modulator (AOM) is utilized so that the heterodyned Fresnel spectrum is shifted from DC by several dozen megahertz; otherwise, the Fresnel reflection spectrum to be detected overlaps with the low-frequency noise of the electrical devices.

Additionally, in order to reduce the cost of the system, we have recently developed a new SOCF-OCDR configuration without using an AOM [29]. By exploiting the foot of the Fresnel reflection spectrum, a sufficiently high signal-to-noise ratio (SNR) was obtained. However, in both the standard and simplified SOCF-OCDR configurations mentioned above, two optical paths—the incident optical path including an FUT and the reference optical path for optical interference—were required. Removing the reference path will further simplify the system and boost its practical convenience.

By using a polymer optical fiber (POF) as an FUT, we have already demonstrated SOCF-OCDR operations without an explicit reference path [30]. In this case, the Fresnel-reflected light generated at the boundary between the POF and a silica single-mode fiber (SMF; a pigtail of an optical circulator) was used as a reference light. However, when the FUT is composed not of a POF but of silica SMF, Fresnel-reflected light is not generated at the boundary of the two silica SMFs, which makes it difficult for us to demonstrate the similar SOCF-OCDR operations.

In this work, we develop a simplified configuration of AOM-free SOCF-OCDR without an explicit reference path when standard silica SMF is used as an FUT. Instead, the Fresnel-reflected light generated at the distal open end of the FUT is exploited as a reference light. In addition to demonstrating the basic operation of this approach, we investigate the optimal incident power and the influence of the loss near the distal end on the measured results.

2. PRINCIPLE AND EXPERIMENTAL SETUP

Figure 1 depicts the experimental setup of the AOM-free SOCF-OCDR without a reference path, which is extremely simple compared to previous configurations [21–29]. The laser output at 1550 nm was amplified using an erbium-doped fiber amplifier (EDFA) and was injected into an FUT composed of sequentially connected multiple silica SMFs (detailed below in this section). The reflected light, which contained the optical beat signal between the light beams reflected at the SMF-to-SMF boundaries and the light beam Fresnel-reflected at the distal open end of the FUT (~4% reflectivity), was guided to a photodetector (note that some structural analogy can be found in optical coherence tomography [31]). The beat signal was then converted into an electrical signal and input to an electrical spectrum analyzer (ESA). By using the ESA as an electrical narrow bandpass filter, the electrical spectral power at 2 MHz (at which a maximal SNR can be obtained [29]) was selectively transmitted to an oscilloscope. The resolution bandwidth and the video bandwidth of the ESA were set to 300 kHz and 1 kHz, respectively.

To perform distributed reflectivity (or reflection power) measurements, the output frequency of the laser was sinusoidally modulated by directly modulating the driving current, leading to the formation of a correlation peak in the FUT [26] (here we denote the modulation frequency and amplitude of the optical frequency by f_m and Δf, respectively). The light reflected at a specific position along the FUT can be selectively observed using the correlation peak. By sweeping the modulation frequency, the correlation peak is scanned along the FUT, and in this manner the reflectivity distribution can be obtained. In a conventional SOCF-OCDR system involving a reference path (either with or without an AOM), sinusoidal frequency modulation generates multiple correlation peaks periodically. The measurement range D is then given by the spacing between the correlation peaks as follows [32],

$$D = \frac{c}{2nf_m}, \tag{1}$$

where c is the velocity of light in a vacuum, and n is the refractive index of the fiber core. The spatial resolution Δz (which equals the 3 dB linewidth of the correlation peak) is theoretically given by [32]

$$\Delta z \cong \frac{0.76c}{\pi n \Delta f}. \tag{2}$$

However, in an SOCF-OCDR system without a reference path, the measurement range D is limited to the proximal half of the FUT length, rather than the range expressed by Eq. (1).

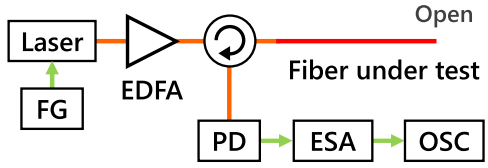

Fig. 1. Experimental setup of simplified optical correlation-domain reflectometry (OCDR) without a reference path. EDFA, erbium-doped fiber amplifier; ESA, electrical spectrum analyzer; FG, function generator; OSC, oscilloscope; PD, photodiode.

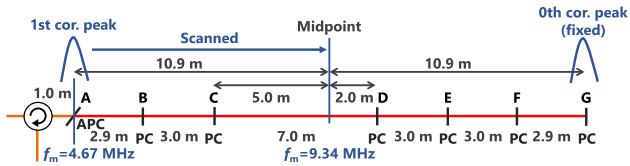

Fig. 2. Schematic structure of the fiber under test (FUT).

This is because in this configuration, the 0th correlation peak—i.e., the zero-optical-path-difference point—is constantly located at the distal open end of the FUT, and the first correlation peak is utilized for distributed measurement. When the first peak reaches the midpoint of the FUT, the second peak starts to enter the FUT at the optical circulator. Note that a similar configuration has been implemented in a Brillouin-based OCDR system [33]. Although the spatial resolution of this simplified Brillouin OCDR is a function of the sensing position, that of the SOCF-OCDR without a reference path is not dependent on the sensing position.

The detailed structure of the FUT is shown in Fig. 2. A 1.0 m long pigtail (silica SMF) of the circulator was sequentially connected to 2.9, 3.0, 7.0, 3.0, 3.0, and 2.9 m long silica SMFs using fiber-channel/physical-contact (FC/PC) or fiber-channel/angled-physical-contact (FC/APC) connectors. The distal PC end of the FUT was kept open. The modulation frequency f_m was swept from 4.67 to 9.34 MHz with a repetition rate of 33 Hz, which corresponds to the measurement range of d = 0–10.9 m (where d was defined as the length between Connector A and the distal end). The modulation amplitude Δf was set to 0.75 GHz (to avoid the damage of the laser), which corresponded to the spatial resolution of 66 mm according to Eq. (2). The range-to-resolution ratio was currently 167, which can be further enhanced by employing a laser specially designed for high-amplitude modulation use, such as a super-structure-grating distributed-Bragg-reflector laser [34,35]. A temporal gating technique [36,37] may be another method for improving the range-to-resolution ratio.

3. EXPERIMENTAL RESULTS

First, the reflection power distributions along the FUT were measured with varying incident power P_{in}, as shown in Fig. 3. When P_{in} was higher than ~0 dBm, clear peaks corresponding to Connectors B and C were observed at d = 2.9 and 5.9 m, respectively, which verified the basic operation of this system. However, when P_{in} was lower than ~0 dBm, the peak corresponding to Connector C was buried by the noise floor.

We then evaluated the P_{in} dependence of the SNR of each peak, which was defined as the ratio between the reflection power and the noise floor at a certain position. As shown in Fig. 4, as P_{in} increased, the SNR became maximal and then decreased for both peaks. Under these experimental conditions, the optimal P_{in} value that yielded the maximal SNR was approximately 8 dBm, irrespective of the connector in question. Another finding is that the measurement was correctly performed with a moderate SNR even when P_{in} was lower than 0 dBm. This indicates that the EDFA is not required in the

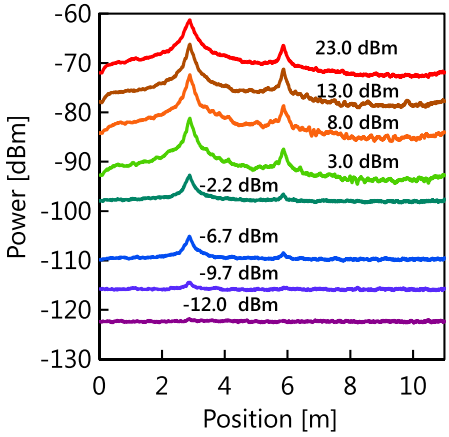

Fig. 3. Measured distributions of reflection power as a function of position for various incident powers.

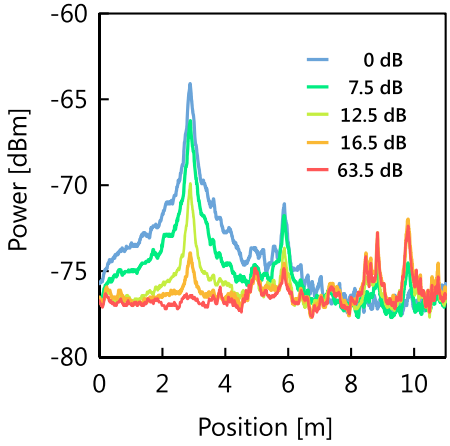

Fig. 5. Measured distributions of reflection power for various bending loss values.

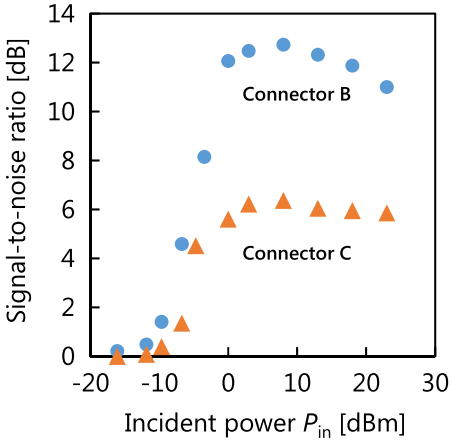

Fig. 4. Signal-to-noise ratio (SNR) measured as a function of the incident power.

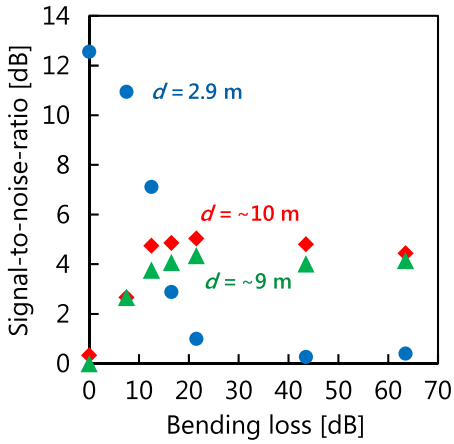

Fig. 6. Signal-to-noise ratio (SNR) measured as a function of the bending loss.

incident path, which is desirable from the standpoint of system simplification.

At this point, we evaluated the influence of the noise caused by the 0th correlation peak. Note that in a Brillouin-based OCDR system without a reference path, some amount of loss must be artificially applied near the distal open end in order to mitigate the influence of the 0th correlation peak, and thus to obtain a sufficiently high SNR [33]. Accordingly, a tunable bending loss was applied to the point 0.1 m away from the distal end. The P_{in} value was 8 dBm. The dependence of the measured reflection power distribution on the bending loss is shown in Fig. 5. As the bending loss increased, the power of the two peaks corresponding to Connectors B and C decreased, while new peaks started to grow at $d = \sim 9$ and ~ 10 m, where no connectors existed. These ghost peaks can be explained by the fact that, as the reflection power from the original 0th correlation peak located at the distal end decreases, one of the SMF-to-SMF boundaries with relatively weak reflectivity starts to function as a new 0th correlation peak; in this manner, the multiple reflections among the connectors result in the appearance of the ghost peaks.

Finally, the bending loss dependence of the SNR (the ghost peaks were also included in the SNR measurements) at $d = 2.9$, ~ 9, and ~ 10 m was measured (Fig. 6). As the bending loss increased, the SNR of the desired peak at $d = 2.9$ m decreased, while those of the ghost peaks increased. This result indicates that, unlike in the case of the Brillouin OCDR system that is based on frequency information, we need not (or should not) apply an artificial loss near the open end in the Fresnel OCDR system that is based on power information.

4. CONCLUSION

A simplified SOCF-OCDR configuration without an explicit reference path was developed. As standard silica SMF was used as an FUT, and the Fresnel-reflected light generated at the distal open end of the FUT was exploited as a reference light. Distributed reflection power measurements were demonstrated, and the optimal incident power was found to be approximately 8 dBm. We also showed that the loss near the distal end should not be applied, unlike in the case of

Brillouin-based OCDR. We believe that although our simplified AOM-free SOCF-OCDR system has a disadvantage that its measurement range is limited to the proximal half of the FUT length, it will still be of great use in implementing cost-efficient distributed reflectivity sensors in the future.

Funding. Japan Society for the Promotion of Science (JSPS) KAKENHI (25709032, 26630180, 25007652).

REFERENCES

1. B. L. Danielson and C. D. Whittenberg, "Guided-wave reflectometry with micrometer resolution," Appl. Opt. **26**, 2836–2842 (1987).
2. Y. Mizuno, W. Zou, Z. He, and K. Hotate, "Proposal of Brillouin optical correlation-domain reflectometry (BOCDR)," Opt. Express **16**, 12148–12153 (2008).
3. T. Kurashima, T. Horiguchi, H. Izumita, S. Furukawa, and Y. Koyamada, "Brillouin optical-fiber time domain reflectometry," IEICE Trans. Commun. **E76-B**, 382–390 (1993).
4. N. Hayashi, Y. Mizuno, and K. Nakamura, "Distributed Brillouin sensing with centimeter-order spatial resolution in polymer optical fibers," J. Lightwave Technol. **32**, 3397–3401 (2014).
5. A. H. Hartog, A. P. Leach, and M. P. Gold, "Distributed temperature sensing in solid-core fibres," Electron. Lett. **21**, 1061–1062 (1985).
6. J. Park, G. Bolognini, D. Lee, P. Kim, P. Cho, F. D. Pasquale, and N. Park, "Raman-based distributed temperature sensor with simplex coding and link optimization," IEEE Photon. Technol. Lett. **18**, 1879–1881 (2006).
7. S. Binu, V. P. M. Pillai, and N. Chandrasekaran, "OTDR based fiber optic microbend sensor for distributed sensing applications in structural pressure monitoring," J. Opt. **35**, 36–44 (2006).
8. A. Kharaz and B. E. Jones, "A distributed optical-fibre sensing system for multi-point humidity measurement," Sens. Actuators A **47**, 491–493 (1995).
9. M. K. Barnoski and S. M. Jensen, "Fiber waveguides: a novel technique for investigating attenuation characteristics," Appl. Opt. **15**, 2112–2115 (1976).
10. G. P. Lees, H. H. Kee, and T. P. Newson, "OTDR system using Raman amplification of a 1.65 μm probe pulse," Electron. Lett. **33**, 1080–1081 (1997).
11. M. Zoboli and P. Bassi, "High spatial resolution OTDR attenuation measurements by a correlation technique," Appl. Opt. **22**, 3680–3681 (1983).
12. P. Healey and P. Hensel, "Optical time-domain reflectometry by photon counting," Electron. Lett. **16**, 631–633 (1980).
13. Q. Zhao, L. Xia, C. Wan, J. Hu, T. Jia, M. Gu, L. Zhang, L. Kang, J. Chen, X. Zhang, and P. Wu, "Long-haul and high-resolution optical time domain reflectometry using superconducting nanowire single-photon detectors," Sci. Rep. **5**, 10441 (2015).
14. W. Eickhoff and R. Ulrich, "Optical frequency domain reflectometry in single-mode fiber," Appl. Phys. Lett. **39**, 693–695 (1981).
15. H. Ghafoori-Shiraz and T. Okoshi, "Fault location in optical fibers using optical frequency domain reflectometry," J. Lightwave Technol. **4**, 316–322 (1986).
16. B. J. Soller, D. K. Gifford, M. S. Wolfe, and M. E. Froggatt, "High resolution optical frequency domain reflectometry for characterization of components and assemblies," Opt. Express **13**, 666–674 (2005).
17. D. Arbel and A. Eyal, "Dynamic optical frequency domain reflectometry," Opt. Express **22**, 8823–8830 (2014).
18. B. Wang, X. Fan, S. Wang, G. Yang, Q. Liu, and Z. He, "Laser phase noise compensation in long-range OFDR by using an optical fiber delay loop," Opt. Commun. **365**, 220–224 (2016).
19. R. C. Youngquist, S. Carr, and D. E. N. Davies, "Optical coherence-domain reflectometry: a new optical evaluation technique," Opt. Lett. **12**, 158–160 (1987).
20. E. A. Swanson, D. Huang, M. R. Hee, J. G. Fujimoto, C. P. Lin, and C. A. Puliafito, "High-speed optical coherence domain reflectometry," Opt. Lett. **17**, 151–153 (1992).
21. K. Hotate, M. Enyama, S. Yamashita, and Y. Nasu, "A multiplexing technique for fibre Bragg grating sensors with the same reflection wavelength by the synthesis of optical coherence function," Meas. Sci. Technol. **15**, 148–153 (2004).
22. Z. He, T. Tomizawa, and K. Hotate, "High-speed high-reflectance-resolution reflectometry by synthesis of optical coherence function," IEICE Electron. Express **3**, 122–128 (2006).
23. Z. He, M. Konishi, and K. Hotate, "A high-speed sinusoidally frequency-modulated optical reflectometry with continuous modulation-frequency sweeping," Proc. SPIE **7004**, 70044L (2008).
24. K. Hotate and O. Kamatani, "Reflectometry by means of optical-coherence modulation," Electron. Lett. **25**, 1503–1505 (1989).
25. Z. He and K. Hotate, "Distributed fiber-optic stress-location measurement by arbitrary shaping of optical coherence function," J. Lightwave Technol. **20**, 1715–1723 (2002).
26. K. Hotate, "Application of synthesized coherence function to distributed optical sensing," Meas. Sci. Technol. **13**, 1746–1755 (2002).
27. Z. He, H. Takahashi, and K. Hotate, "Optical coherence-domain reflectometry by use of optical frequency comb," in *Conference on Lasers and Electro-Optics (CLEO)*, San Jose, CA (IEEE, 2010), paper CFH4.
28. H. Takahashi, Z. He, and K. Hotate, "Optical coherence domain reflectometry by use of optical frequency comb with arbitrary-waveform phase modulation," in *36th European Conference and Exhibition on Optical Communication*, Torino (IEEE, 2010), paper Tu.3.F.4.
29. M. Shizuka, S. Shimada, N. Hayashi, Y. Mizuno, and K. Nakamura, "Optical correlation-domain reflectometry without optical frequency shifter," Appl. Phys. Express **9**, 032702 (2016).
30. N. Hayashi, M. Shizuka, K. Minakawa, Y. Mizuno, and K. Nakamura, "Simplified optical correlation-domain reflectometry using polymer fiber," IEICE Electron. Express **12**, 20150824 (2015).
31. U. Sharma, N. M. Fried, and J. U. Kang, "All-fiber common-path optical coherence tomography: sensitivity optimization and system analysis," IEEE J. Sel. Top. Quantum Electron. **11**, 799–805 (2005).
32. K. Hotate and K. Kajiwara, "Proposal and experimental verification of Bragg wavelength distribution measurement within a long-length FBG by synthesis of optical coherence function," Opt. Express **16**, 7881–7887 (2008).
33. N. Hayashi, Y. Mizuno, and K. Nakamura, "Simplified configuration of Brillouin optical correlation-domain reflectometry," IEEE Photon. J. **6**, 6802807 (2014).
34. H. Ishii, H. Tanobe, F. Kano, Y. Tohmori, Y. Kondo, and Y. Yoshikuni, "Quasicontinuous wavelength tuning in super-structure-grating (SSG) DBR lasers," IEEE J. Quantum Electron. **32**, 433–441 (1996).
35. Z. He and K. Hotate, "Synthesized optical coherence tomography for imaging of scattering objects by use of a stepwise frequency-modulated tunable laser diode," Opt. Lett. **24**, 1502–1504 (1999).
36. M. Kannou, S. Adachi, and K. Hotate, "Temporal gating scheme for enlargement of measurement range of Brillouin optical correlation domain analysis for optical fiber distributed strain measurement," in *Proceedings of 16th International Conference on Optical Fiber Sensors*, Nara, Japan (2003), pp 454–457.
37. Y. Mizuno, Z. He, and K. Hotate, "Measurement range enlargement in Brillouin optical correlation-domain reflectometry based on temporal gating scheme," Opt. Express **17**, 9040–9046 (2009).